Observation of electric-quadrupole infrared transitions in water vapor

Alain Campargue, Samir Kassi, Andrey Yachmenev, Aleksandra A Kyuberis, Jochen Küpper, Sergei N Yurchenko

Observation of electric-quadrupole infrared transitions in water vapour

Alain Campargue[a *], Samir Kassi[a], Andrey Yachmenev [b,c],
Aleksandra A. Kyuberis[d], Jochen Küpper[b,c,e], Sergei N. Yurchenko[f]

[a] *Univ. Grenoble Alpes, CNRS, LIPhy, 38000 Grenoble, France*
[b] *Center for Free-Electron Laser Science, Deutsches Elektronen-Synchrotron DESY, Notkestraße 85, D-22607 Hamburg, Germany*
[c] *Center for Ultrafast Imaging, Universität Hamburg, Luruper Chaussee 149, 22761 Hamburg, Germany*
[d] *Institute of Applied Physics, Russian Academy of Sciences, Ulyanov Street 46, Nizhny Novgorod, Russia 603950*
[e] *Department of Physics, Universität Hamburg, Luruper Chaussee 149, 22761 Hamburg, Germany*
[f] *Department of Physics and Astronomy, University College London, London, WC1E 6BT, UK*

Key words: electric-quadrupole transitions, absorption spectroscopy, water, cavity ring down spectroscopy

Number of Pages: 15
Number of Figures: 4
Number of Tables: 2

Corresponding author.
E-mail address: alain.campargue@univ-grenoble-alpes.fr
Tel.: 33 4 76 51 43 19 Fax. 33 4 76 63 54 95

Molecular absorption of infrared radiation is generally due to ro-vibrational electric-dipole transitions. Electric-quadrupole transitions may still occur, but they are typically a million times weaker than electric-dipole transitions, rendering their observation extremely challenging. In polyatomic or polar diatomic molecules, ro-vibrational quadrupole transitions have never been observed. Here, we report the first direct detection of quadrupole transitions in water vapor. The detected quadrupole lines have intensity largely above the standard dipole intensity cut-off of spectroscopic databases and thus are important for accurate atmospheric and astronomical remote sensing.

Spectroscopic techniques in the IR domain have advanced significantly in recent years providing exciting opportunities for new generation of accurate and sensitive measurements. Quadrupole electronic and ro-vibrational transitions have been detected in a number of atoms [1,2] and homonuclear diatomic molecules [3,4,5], respectively, for states that cannot undergo electric dipole transitions. Electric-quadrupole transitions are used for remote sensing of important diatomic molecules, such as hydrogen, oxygen, and nitrogen, in spectra of Earth's atmosphere and other environments [4,6,7]. When compared with dipole transitions, quadrupole transition rates are typically smaller by a factor ranging from 10^8 in the IR to 10^5 in the optical spectral domain. Such extremely long mean lifetimes against spontaneous emission of quadrupole excitations make them ideal candidates for next-generation atomic clocks [8], high-precision tests of molecular physics [9,10,11], and quantum information processing [8,12].

In most heteronuclear diatomic and polyatomic molecules the ro-vibrational states can be excited both *via* dipole and quadrupole transitions. The dipole and quadrupole moment operators have distinct selection rules. The dipole moment connects states with different parity, while for the quadrupole transitions, the parity is conserved. Furthermore, states with rotational quantum numbers J differing by ±2 can only be connected by a quadrupole transition. This difference in selection rules permits, in principle, the observation of well-isolated quadrupole lines. Nevertheless, in practice the detection of quadrupole lines is made difficult by the fact that, even if transition frequencies differ, the quadrupole lines are drowned in the line profile of the much stronger dipole lines.

To the best of our knowledge, quadrupole transitions have never been detected in polyatomic molecules until now, although the quadrupole moment of some polyatomic molecules (CO_2, NO_2, OCS) have been measured using electric-field-gradient-induced birefringence method [13]. Nowadays, spectroscopic line lists of the major greenhouse gas absorbers such as water vapour and carbon dioxide, are limited to dipole transitions [14]. A highly-accurate and complete characterization of ro-vibrational spectra of these molecules is needed for the modeling and understanding of Earth's atmosphere, climate, and many remote sensing experiments [15]. At present, adequate models of the water vapour absorption in the Earth's atmosphere incorporate many weak dipole lines including hot band transitions, minor water isotopologues contribution, and weak absorption continua [16]. Obviously, failure to include weak quadrupole transitions to the total opacities of atmospherically

important species may contribute to systematic errors in remote sensing retrievals with a corresponding impact on atmospheric simulations.

Here, we report the first observation of electric-quadrupole transitions in water vapour. This is actually the first time that quadrupole lines of a polyatomic molecule have been detected in an IR spectrum. This observation was made possible using a continuous wave diode laser cavity ring down spectroscopic (CRDS) technique to measure the water absorption spectrum near 1.3 μm. The detection and assignment of the measured spectral lines relied on high-accuracy predictions for both positions and intensities of the quadrupole $H_2{}^{16}O$ transitions. It is important to stress that the detected quadrupole lines have intensity largely above the recommended dipole intensity cut-off of the standard spectroscopic databases and should thus be incorporated.

CRDS is a high-sensitivity absorption technique which performs like a classical absorption spectroscopy that would have a multi-kilometric absorption path-length. The method consists in measuring the power decay rate (ring down) of a laser light trapped into a passive optical cavity, made of high-reflectivity semi-transparent mirrors [17]. The presence of an absorbing gas in the cavity shortens the ring down time. From the variation of the decay rate with the laser frequency, one gets the absorption spectrum. Because of the extreme reflectivity of the mirrors (typically R~99.997 %) sensitivities equivalent to several hundred kilometers in a classical absorption approachareroutinely achieved and extremely weak absorptions are detected. A record absorption sensitivity, $\alpha_{min} \approx 5\times10^{-13}$ cm^{-1}, corresponding to a 2% light attenuation for the Earth-Moon distance, was achieved by CRDS [18], allowing for the detection of extremely weak quadrupole lines of D_2 and N_2 [19]. In the last two decades, the CRDS technique was extensively used to characterize weak dipole transitions of water vapour in the near-IR spectral domain [20]. Tens of thousands of new dipole transition lines were detected and assigned to various water isotopologues present in natural isotopic abundance. In the 1.6 and 1.25 μm transparency windows, lines of $HD^{17}O$ with a natural relative abundance of 1.158×10^{-7} were detected [21] and dipole lines with intensities as weak as 1×10^{-29} cm/molecule were measured [22].

At room temperature and typical sample cell pressures in the Torr range, most of quadrupole transitions of water molecule are masked by much stronger dipole transitions. In order to detect them in the CRDS spectrum, a highly accurate theoretical prediction of the quadrupole ro-vibrational spectrum is essential.

The calculations, detailed in **Appendix A**, employed a state-of-the-art variational approach based on high-level *ab initio* electric dipole and quadrupole moment surfaces of H_2O. The robust variational approach TROVE [23,24] was used to solve the ro-vibrational Schrödinger equation for the motion of nuclei, based on exact kinetic energy operator [25,26] and recently reported accurate potential energy surface of H_2O [25]. The electric-quadrupole moment surface was computed *ab initio* at the CCSD(T)/aug-cc-pVQZ level of theory in the frozen-core approximation using the CFOUR

program package [26]. The quadrupole intensities and Einstein *A* coefficients were calculated using the generalized approach RichMol for molecular dynamics in the presence of external electric fields [27]. The basis-set convergence of the ro-vibrational line positions was carefully examined. The remaining errors on the order of 0.01 - 0.6 cm^{-1} were still too significant to unambiguously identify quadrupole lines in the CRDS spectrum. To improve the accuracy, the computed ro-vibrational line positions were adjusted according to empirical values of the lower and upper state energy levels of $H_2{}^{16}O$. These energies were carefully derived from the analysis of high-resolution spectroscopic data from more than a hundred experimental sources [28]. The average uncertainties on the order 10^{-3} cm^{-1} in the resulting line centers allowed to unambiguously identify quadrupole lines. Indeed, in the region of interest, with the sensitivity of the CRDS spectra under analysis, the spectral congestion is very high, due to dipole lines of $H_2{}^{16}O$, water minor isotopologues, as well as impurities such as CO_2, NH_3 or CH_4 present at ppm relative concentrations.

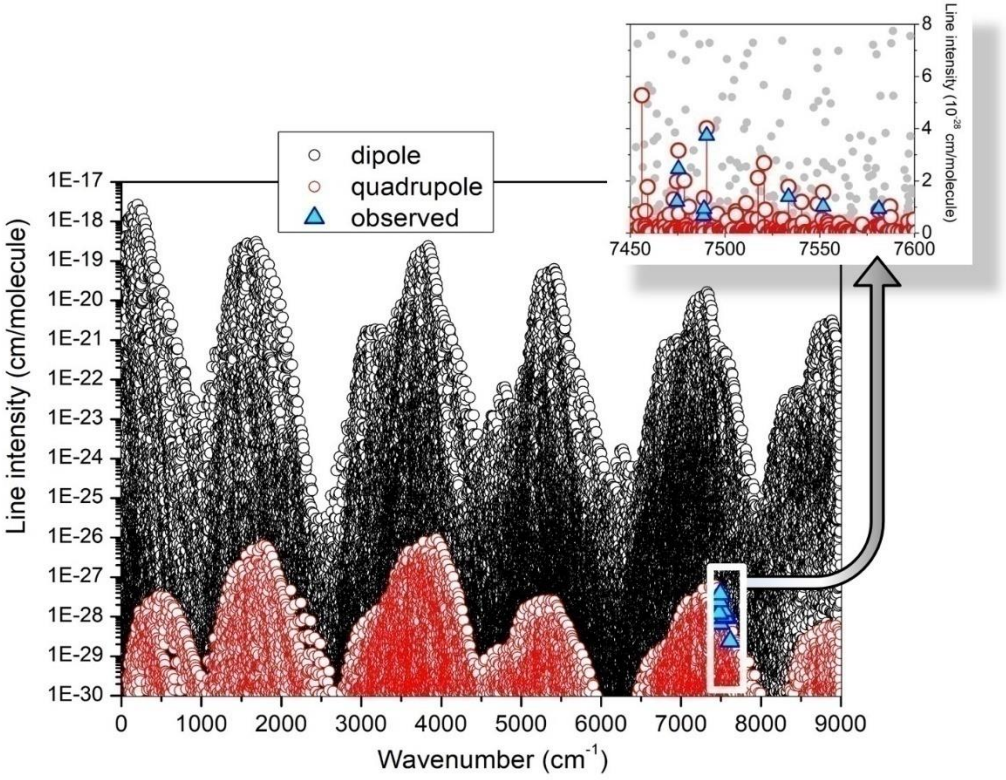

FIG. 1 Overview of the absorption line list of $H_2{}^{16}O$ at 296 K. The calculated electric-quadrupole spectrum [29] (red circles) is superimposed to the calculated electric-dipole spectrum (black circles). The CRDS measured quadrupole transitions are shown with blue triangles. The insert with intensities in linear scale shows a zoom of the 7450-7600 cm^{-1} region.

The overview of the calculated quadrupole line list of $H_2{}^{16}O$ [29] is displayed shown in **Fig. 1** superimposed to the dipole line list computed using an *ab initio* dipole moment surface [30]. Both lists include all ro-vibrational transitions of $H_2{}^{16}O$ with $J \leq 30$ and upper state energies below 10000 cm^{-1} with respect to the zero-point level. The general appearance of the quadrupole and dipole line lists is similar; the spectra consist of a succession of vibrational bands whose intensity decreases with the

frequency. The maximum intensity values of quadrupole lines are typically seven orders of magnitude smaller than the dipole lines. Note that the strongest quadrupole lines near 4000 cm^{-1} have an intensity on the order of 10^{-26} cm/molecule while the intensity cut off the water dipole transitions included in the HITRAN database [14] is three orders of magnitude smaller (10^{-29} cm/molecule). Interestingly, the largest quadrupole-to-dipole intensity ratios of about 10^{-4} are predicted for the water transparency window at 2500 cm^{-1}, dominated by transitions of the bending ν_2 vibrational band. The complete quadrupole line list with transition frequencies up to10000 cm^{-1} and 10^{-40} cm/molecule intensity cut-off is provided as Supplemental Material [29].

The CRDS recordings of natural water vapour were performed in the frequency range between 7408 and 7619 cm^{-1} at a pressure limited to 1.0 Torr and temperature maintained at 296 K. Details about the experimental setup and line parameters retrieval can be found in **Appendix B**. The noise equivalent absorption of the recordings, estimated as a root-mean-square deviation of the spectrum base line, is $\alpha_{min} \approx 5\times10^{-11}$ cm^{-1}. In terms of line intensity, this converts to a detectivity threshold on the order of few 10^{-29} cm/molecule, well below the calculated intensities of the strongest quadrupole lines in the region (up to 6×10^{-28} cm/molecule).

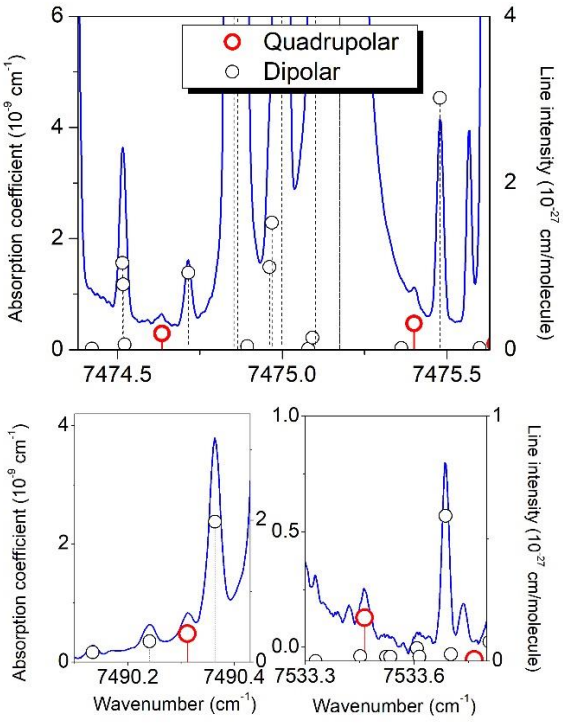

FIG. 2. Detection of electric-quadrupole lines of $H_2{}^{16}O$ in the spectrum of water vapour recorded by CRDS at 1.0 Torr. The quadrupole spectrum of $H_2{}^{16}O$ (red stars) calculated in this work is superimposed to the dipole stick spectrum of water in natural isotopic abundance [14] (blue circles). The four detected quadrupole lines correspond to ΔJ= 2 transitions of the $\nu_1+\nu_3$ band.

As illustrated on **Fig. 2**, the remarkable position and intensity coincidences of the calculated quadrupole lines to the recorded spectra leaves no doubt that $H_2{}^{16}O$ quadrupole lines are detected. Among the fifty quadrupole lines predicted with sufficient intensity in the considered region, nine could be detected (blue triangles in **Fig. 1)**, the others being hidden by stronger dipole lines. As a result, **Table 1** lists the detected quadrupole lines with their measured positions and intensities

obtained from the line profile fit described in **Appendix B**. The rovibrational assignments included in the table indicate that the detected lines belong to the $\nu_1+\nu_3$ band and correspond to $\Delta J = 2$ transitions except one line corresponding to $\Delta J = 1$. Experimental intensity values show a reasonable agreement with the calculated values (see insert in **Fig. 1**). Excluding the two weakest lines with large experimental uncertainties, the average measured/computed intensity ratio is 0.80(17).

Position (cm^{-1})		Int. (cm/molecule)		$J\ K_a\ K_c$					
Meas.	Calc.	Meas.	Calc.	Upper level			Lower level		
7474.6325	7474.6354	1.21E-28	1.98 E-28	6	1	5	4	2	3
7475.4020	7475.4005	2.46E-28	3.16 E-28	5	2	4	3	1	2
7488.5747	7488.5785	6.72E-29	3.23 E-29	6	6	1	5	5	0
7488.9183	7488.9215	9.34E-29	1.34 E-28	7	0	7	5	1	5
7490.3117	7490.3120	3.74E-28	4.02 E-28	7	1	7	5	0	5
7533.4649	7533.4642	1.39E-28	1.72 E-28	7	2	6	5	1	4
7551.7653	7551.7639	1.02E-28	1.56 E-28	9	1	9	7	0	7
7581.1247	7581.1172	9.32E-29	8.53 E-29	10	0	10	8	1	8
7613.8512	7613.8478	2.37E-29	1.10 E-29	10	2	9	8	1	7

Table 1
Assignment, transition frequencies, and intensities of the electric-quadrupole lines of the $\nu_1+\nu_3$ band of $H_2{}^{16}O$ measured near 1.3 μm.

This first detection of quadrupole transitions in the water vapour spectrum opens new perspectives for theoretical and experimental absorption spectroscopy of polyatomic molecules with expected impact in atmospheric and astronomical sciences. Despite being very weak, quadrupole absorption lines of water vapour are clearly above the background formed by the dipole spectrum and the water continuum and therefore must be included into modern atmospheric databases such as HITRAN [14] or ExoMol [31]. Water vapour, being one of the major interfering species for the trace gas analysis in air, missing quadrupole transitions may skew the optical measurement of the targeted species. In geosciences, small, but measurable natural variation of abundance ratios of water minor isotopologues are used to trace various chemical and physical processes. In this context, absorption spectroscopy is an emerging method with specific advantages compared to conventional mass spectrometers [32-35]. Due to the small relative abundance of the minor isotopologues (2×10^{-3} for $H_2{}^{18}O$ and less than 4×10^{-4} for HDO and $H_2{}^{17}O$), their absorption lines are weak and any accidental coincidence between the target absorption line of the water minor isotopologue and an E2 line of the main isotopologue ($H_2{}^{16}O$) will bias the retrieved abundances.

Similar biases may be encountered for metrological spectroscopic measurements of line intensities or line shapes e.g. in the determination of the Boltzmann constant by Doppler-broadening thermometry of a water line [36].

In the case of water vapour the envelopes of the strong quadrupole and dipole vibrational bands mostly coincide as a result of molecular symmetry and corresponding selection rules. This will not be the case in other important atmospheric species such as CO_2 where, due to the linear structure of the molecule, different selection rules apply to quadrupole and dipole bands. Relatively strong quadrupole

bands may be located in spectral regions where dipole absorption is weak, the so-called transparency windows. In these cases, the importance of quadrupole transitions will even be more apparent.

This study paves the way to systematic computation of quadrupole spectra for all standard atmospheric molecules, *e.g.*, CO_2, N_2O, CH_4, HCN, CO, HF. Owing to the weak character of the quadrupole spectra, systematic calculations across wide spectral range are thus required to evaluate the significance of quadrupole transitions for atmospheric, astrophysical, and industrial applications. After validation tests by high-sensitivity measurements, quadrupole transitions should be systematically incorporated into the most currently used spectroscopic databases.

APPENDIX A: ELECTRONIC STRUCTURE CALCULATION

For water molecule in $C_{2v}(M)$ molecular symmetry group, the rank-2 quadrupole-moment tensor Q transforms as $3A_1 + A_2 + B_1 + B_2$, where A_2 and B_1 components are zero and only two out of three A_1-symmetry components are necessary, because the quadrupole tensor is traceless, i.e., $Q_{A_1}^{(1)} + Q_{A_1}^{(2)} + Q_{A_1}^{(3)} = 0$. In total, three symmetry-adapted components are sufficient to describe the traceless quadrupole tensor of water, these can be constructed as

$$Q_{A_1}^{(i)} = \sum_{\alpha,\beta=x,y,z} S_{i,\alpha} S_{i,\beta} Q_{\alpha,\beta} \qquad \text{for } i = 1,2, \tag{1}$$

$$Q_{B_1} = \sum_{\alpha,\beta=x,y,z} S_{1,\alpha} S_{2,\beta} Q_{\alpha,\beta},$$

where

$$\boldsymbol{S}_i = \frac{r_{\mathrm{H}_i} - r_{\mathrm{O}}}{r_{\mathrm{OH}_i}}, \tag{2}$$

$Q_{\alpha,\beta}$ denotes Cartesian components of the quadrupole moment tensor, and $r_{\mathrm{OH_i}}$ is the $\mathrm{O-H_i}$ bond distance. The quadrupole moment tensor for water was computed ab initio at the CCSD(T)/aug-cc-pVQZ [37,38] level of theory in the frozen-core approximation. Calculations were performed on a grid of about 2000 different molecular geometries covered the wavenumber energy range up to 30 000 cm^{-1} above the equilibrium energy. Analytic CCSD(T) gradient method was used [39], as implemented in the CFOUR program package [26]. The symmetrized components in Eq. (3), were parametrized using fourth order symmetry-adapted power series expansions through least-squares fittings.

Ro-vibrational energies and wavefunctions

The variational TROVE program [23] has been used to solve the ro-vibrational Schrödinger equation for H_2O in its ground electronic state. A new implementation of the exact kinetic energy (EKE) operator developed for this study was used. The EKE is based on the bisector embedding for triatomic molecules [40,41]. Accurate potential energy surface [42], electric dipole moment surface [30] and electric-quadrupole moment surface (this work) were employed.

TROVE uses a multi-layer contraction scheme (see, for example, [43]). At step 1, stretching and bending primitive basis functions are constructed numerically by solving the corresponding 1D

Schrödinger equations. The two equivalent stretching equations are solved on a grid of 2000 points using the Numerov-Cooley approach [44,45]. For the bending solution, the associated Laguerre polynomials are used, which are optimized for the corresponding 1D Schrödinger equation on a grid of 3000 points. The bending 1D Hamiltonian includes the k^2-depended centrifugal distortion term. The details of the model will be published elsewhere [46]. The model 1D Hamiltonian for a given mode (stretch or bend) is constructed by setting the other mode to its equilibrium value. At step 2 the 1D basis functions are then used to solve two reduced problems for the 2D stretching and 1D bending reduced Hamiltonians variationally constructed by averaging the 3D vibrational (J= 0) Hamiltonian over the ground state basis functions as follows:

$$\widehat{H}^{(2D)} = \langle 0_3 | \widehat{H} | 0_3 \rangle, \quad (3)$$

$$\widehat{H}^{(1D)} = \langle 0_1 0_2 | \widehat{H} | 0_1 0_3 \rangle, \quad (4)$$

Where $|v_i\rangle$ band are the stretching (i=*1,2*) and bending (i=*3*) vibrational basis functions with $v = 0$.

The eigenfunctions of these problems are symmetrized using an automatic symmetry adaptation technique [24] and form a 3D vibrational basis set for the $J = 0$ Hamiltonian for step 3. The $C_{2v}(M)$ molecular group symmetry is used to classify the irreducible representations. The eigenfunctions of the ($J = 0$) 3D Hamiltonian are then used to form a ro-vibrational basis set for all $J > 0$ calculations, where the rotational part is constructed from symmetrized rigid rotor functions [24]. Our primitive basis set comprised 18 and 48 functions for the stretching and bending modes, respectively. The atomic masses were used. An E/hc = 40000 cm^{-1} energy cut-off was used to contract the $J = 0$ eigenfunctions. All energies and eigenfunctions up to $J = 30$ were generated and used to produce dipole and quadrupole line lists for water. The final TROVE eigenfunctions are given in a sum-of-product form:

$$|J, m_J, l\rangle = \sum_{v,k} c_{v,k}^{(J,l)} |v\rangle |J, m_J, k\rangle, \quad (5)$$

Where m_J is a projection of the angular momentum on the laboratory Z-axis, k is a projection on the molecularz-axis,l is a counting state number, v is a generic vibrational ($J = 0$) quantum number and $c_{v,k}^{(J,l)}$ is an expansion eigen-coefficient. In order to improve the calculated line positions, empirical energies of $H_2{}^{16}O$ [28] of $H_2{}^{16}O$ were used to replace the TROVE energies where available. In this replacement we took advantage of the two-file structure of the ExoMol line list consisting of a states file and a transition file [31,47].

As an illustration of the quality of the present calculations, **Table 2** shows a comparison of the calculated energy term values (before substitution) with the experimental IUPAC values [28]. The differences can be attributed to the artefacts of the conversion of the empirical PES of H_2O [42] to the analytical representation used in TROVE.

Table 2. Comparison of empirical (Obs.) [28] and calculated (Calc.) energy term values of $H_2{}^{16}O$ (in cm^{-1}) up to 9000 cm^{-1}.

v_1 v_2 v_3	Obs. (cm^{-1})	Calc. (cm^{-1})	Obs.-Calc. (cm^{-1})	v_1	v_2	v_3	Obs. (cm^{-1})	Calc. (cm^{-1})	Obs.-Calc. (cm^{-1})
0 0 0	0.000	0.000	0.000	2	0	0	7249.817	7250.459	-0.642
0 0 1	1594.746	1594.748	-0.002	1	1	0	7445.366	7445.366	0.000
0 0 2	3151.630	3151.640	-0.010	0	0	5	7542.372	7542.423	-0.050
1 0 0	3657.053	3657.159	-0.106	1	0	3	8273.976	8274.070	-0.094
0 1 0	3755.929	3756.058	-0.129	0	1	3	8373.851	8373.952	-0.101
0 0 3	4666.790	4666.789	0.001	0	2	1	8761.582	8762.077	-0.495
1 0 1	5234.976	5235.077	-0.101	2	0	1	8806.999	8807.549	-0.550
0 1 1	5331.267	5331.374	-0.107	0	0	6	8869.950	8870.160	-0.210
0 0 4	6134.015	6134.017	-0.002	1	1	1	9000.410	9000.410	0.000
1 0 2	6775.094	6775.186	-0.093	1	0	4	9724.313	9724.313	0.000
0 1 2	6871.520	6871.622	-0.102	0	1	4	9833.583	9833.686	-0.103
0 2 0	7201.540	7202.099	-0.559						

Quadrupole spectrum simulations

The quadrupole spectrum has been simulated using the variational approach RichMol [27,48], designed for calculations of molecular ro-vibrational dynamics in the presence of external electromagnetic fields. The transition probability due to the electric-quadrupole interaction from a set of $(\boldsymbol{2J+1})$-degenerate initial ro-vibrational states $|\boldsymbol{J,m,l}\rangle$ into a setof $(\boldsymbol{2J'+1})$-degenerate final ro-vibrational states $|\boldsymbol{J',m',l'}\rangle$is given by

$$\boldsymbol{P_Q(J',l'\leftarrow J,l)=\sum_{m'=-J'}^{J'}\sum_{m=-J}^{J}\sum_{A,B=X,Y,Z}\left|\langle J',m',l'|Q_{A,B}|J,m,l\rangle\right|^2}. \quad (6)$$

The ro-vibrational matrix elements of traceless quadrupole tensor operator $Q_{A,B}$ in the laboratory frame $(A,B=X,Y,Z)$ can generally be represented in a contracted tensor form

$$\langle J',m',l'|Q_{A,B}|J,m,l\rangle = M_{A,B}^{(J',m',J,m)}K^{(J',l',J,l)},$$

with

$$M_{A,B}^{(J',m',J,m)}=(-1)^{m'}\sqrt{(2J+1)(2J'+1)}\sum_{\sigma=-2}^{2}[U]_{A,B,\sigma}^{-1}\begin{pmatrix}J & 2 & J'\\ m & \sigma & -m'\end{pmatrix} \quad (7)$$

and

$$K^{(J',l',J,l)}=\sum_{k',v'}\sum_{k,v}\left[c_{v',k'}^{(J',l')}\right]^*\left[c_{v,k}^{(J,l)}\right](-1)^{k'}\sum_{\sigma=-2}^{2}\sum_{\alpha,\beta=x,y,z}\begin{pmatrix}J & 2 & J'\\ k & \sigma & -k'\end{pmatrix}U_{\sigma,\alpha\beta}\langle v'|Q_{\alpha,\beta}|v\rangle. \quad (8)$$

Here, matrix U defines the transformation of the traceless symmetric rank-2 tensor from Cartesian to spherical tensor form (see, e.g., Table I in [27] for explicit expression). The ro-vibrational wavefunction coefficients $c_{v,k}^{(J,l)}$ and vibrational matrix elements of quadrupole tensor operator $\langle v'|Q_{\alpha,\beta}|v\rangle$ in the molecular frame were calculated using TROVE approach, as described in the

previous section. Using Eqs. 8-10, the expression for the ro-vibrational transition probability (in Eq. 8) can be derived as

$$P_Q(J',l' \leftarrow J,l) = \left[K^{(J',l',J,l)}\right]^2 \sum_{m'=-J'}^{J'} \sum_{m=-J}^{J} \sum_{A,B=X,Y,Z} \left|M_{A,B}^{(J',m',J,m)}\right|^2 = \quad (9)$$

$$= 3.8(2J+1)(2J'+1)\left[K^{(J',l',J,l)}\right]^2.$$

The expression for the integrated absorption coefficient of the quadrupole transition inunits cm/molecule reads as

$$I_Q(J',l' \leftarrow J,l) = \frac{4\pi^5 \nu^5 e^{-\frac{E_{J,l}}{kT}}\left(1-e^{-\frac{hc\nu}{kT}}\right)}{(4\pi\epsilon_0)5hcZ(T)} P_Q(J',l' \leftarrow J,l), \quad (10)$$

Where $\nu = (E_{J',l'} - E_{J,l})/hc$ is the transition frequency with $E_{J',l'}$ and $E_{J,l}$ being upper and lower state energies, respectively, and $Z(T)$ is the partition function. Here we used the value of $Z(T$ = 296 K)= 174.5813.

APPENDIX B: CRDS SETUP AND LNE PARAMTER RETRIVIAL

The CRDS spectrum of water at room temperature was recorded from 7408 to 7619 cm^{-1} with a fibred CRDS spectrometer using distributed feed-back (DFB) diode lasers as light sources. A sketch of the experimental arrangement is presented in **Fig. 1**. The stainless steel high finesse cell (HFC) (l= 1.42 m, Φ_{in}= 11.7 mm) is fitted by a pair of supermirrors (~99.998% reflectivity) giving rise to ring down times on the order of 200 μs. The whole spectral region was continuously covered by means of six fibered DFB lasers. The latter were supplied with a constant current of 140 mA, tuned over about 35 cm^{-1} by a temperature sweep of -10 to 60°C. About 40 ring down events were averaged for each spectral data point, distant by approximately 2×10^{-3} cm^{-1}. A complete DFB temperature scan was achieved within 65 minutes. Each time a longitudinal mode of the HFC was excited by the laser frequency, an exponential ring down (RD) event was induced by switching off the laser beam using an acousto-optic modulator (AOM). In order to excite the HFC mode whatever the laser frequency, the HFC length was modulated over one free spectral range by a piezo tube supporting the output mirror [17]. RD times, τ, were measured by fitting with a purely decreasing exponential function the transmission signal measured with an InGaAs photodiode. The obtained loss rate, $1/c\tau$, is the sum of the loss rate of the evacuated cell, $1/c\tau_0$, and of the absorption coefficient, $\alpha(\nu)$, of the gas:

$$\frac{1}{c\tau(\nu)} = \frac{1}{c\tau_0(\nu)} + \alpha(\nu) \quad (11)$$

where c is the speed of light.

The spectra were recorded at 1.0 Torr. The pressure was continuously monitored by a capacitance gauge (Baratron) and the temperature was stabilized at about 296 K. Each 35 cm^{-1} wide

spectrum, corresponding to one DFB recording, was calibrated independently on the basis of the wavenumber values provided by a Fizeau type wavemeter (WSU-30 Highfinesse, 5 MHz resolution and 20 MHz accuracy). The calibration was checked and refined using reference line positions of H_2O from the HITRAN database [14].

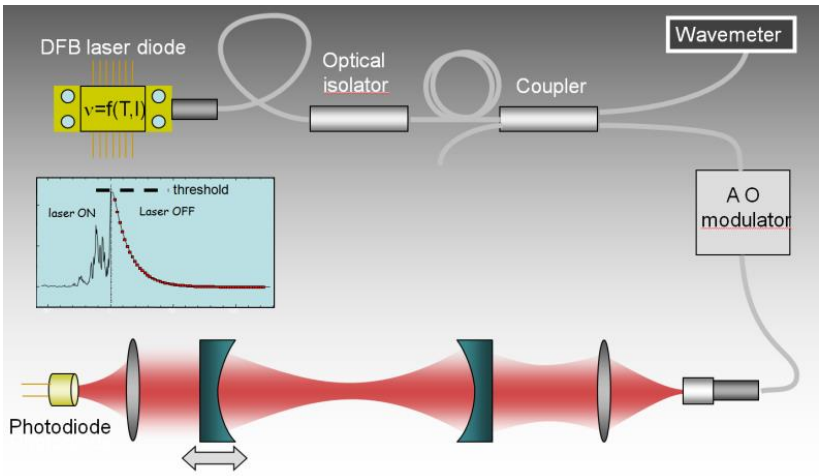

FIG 3. Scheme of the CRD spectrometer. The different components include a distributed feed-back diode laser (DFB), an optical isolator, a fiber coupler, an acousto-optic (AO) modulator and a photodiode. The insert shows the time dependence of the light intensity measured by the photodiode: after a build-up period, the light intensity reaches a threshold value which triggers the switch off of the AO modulator. The ring down time is then measured from the exponential decay of the light intensity.

The line centers and line intensities were obtained by using a homemade interactive least squares multi-lines fitting program written in LabVIEW. As the DFB line width (due to the frequency jitter) is much smaller than the Doppler broadening (1-5 MHz compared to 1 GHz), the contribution of the apparatus function to the observed profiles was neglected. The line parameter derivation consisted in choosing narrow spectral intervals with (overlapping) lines which could be fitted independently. For each interval, line centers, integrated absorption coefficients, the Lorentzian contribution of each line and a baseline (assumed to be a quadratic function of the wavenumber) were provided by the fitting procedure. The Doppler broadening was fixed according the mass and temperature of the gas and the pressure broadening was fixed according to the HITRAN default value of the self-pressure broadening coefficient (0.40 cm^{-1}/atm). **Fig. 4** illustrates the achieved spectrum reproduction close to the noise level for two E2 lines.

The line intensity, S_{ν_0} of a ro-vibrational transition centered at ν_0, was obtained from the integrated absorption coefficient, A_{ν_0}(cm^{-2}/molecule):

$$A_{\nu_0} = \int_{line} \alpha_\nu \, d\nu = S_{\nu_0}(T)N \qquad (12)$$

Where ν is the wavenumber in cm^{-1}, α_ν is the absorption coefficient in cm^{-1} obtained from the cavity ring down time (Eq. 2) and N is the molecular concentration in molecule/cm^3 obtained from the measured pressure and temperature values: $P = NkT$.

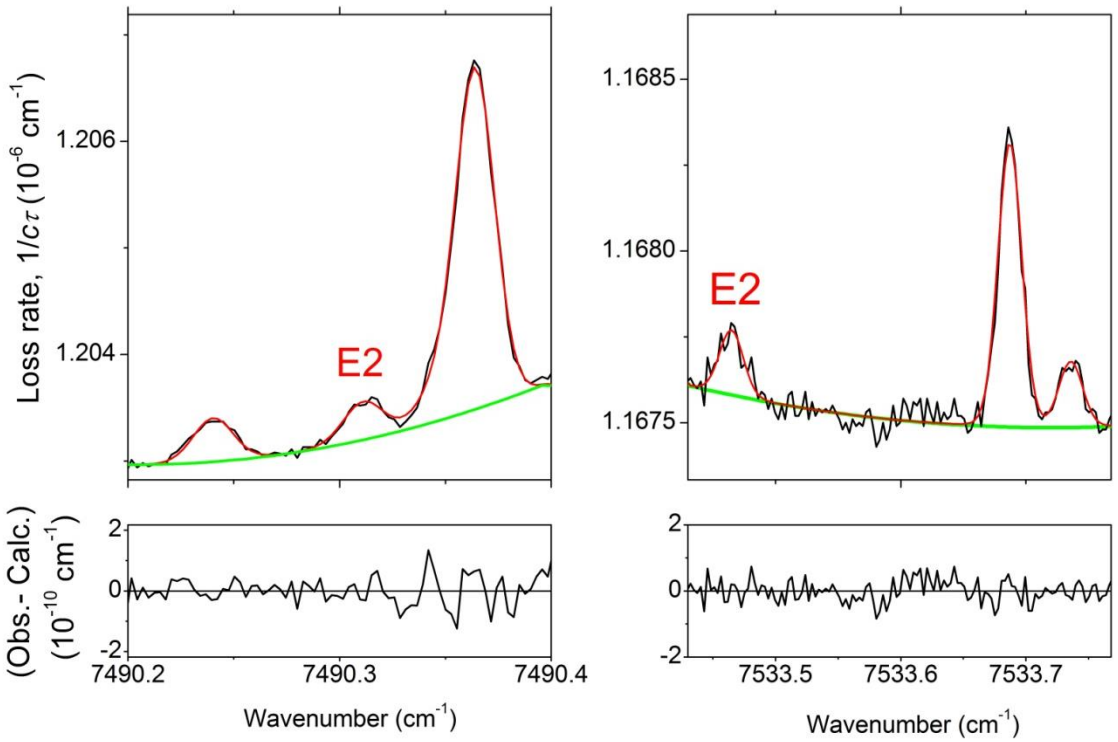

FIG 4. Examples of line profile fitting for the quadrupolar (E2) lines of $H_2{}^{16}O$ at 7490.311 and 77533.4649 cm^{-1}. The lower panels show the difference between the CRDS (black) and fitted (red) spectra in 10^{-10} cm^{-1} units. The green curve corresponds to the fitted baseline assumed to be a quadratic polynomial of the wavenumber.

The retrieved centers and intensities of the nine quadrupolar lines are given in Table 1. As a result of the weakness of the considered lines and strong line overlapping, the error bars on the fitted line centers are estimated to be $2\text{-}3\times10^{-3}$ cm^{-1} while the uncertainty on the experimental intensities ranges between 20 and 60 %.

ACKNOWLEDGMENTS

SY acknowledges support from the UK Science and Technology Research Council (STFC) No. ST/R000476/1. A substantial part of the calculations was performed using high performance computing facilities provided by DiRAC for particle physics, astrophysics and cosmology and supported by BIS National E-infrastructure capital grant ST/J005673/1 and STFC grants ST/H008586/1, ST/K00333X/1. The work of AAK was supported by the Foundation for the Advancement of Theoretical Physics and Mathematics BASIS. The work of A.Y. and J.K. has been supported by the Deutsche Forschungsgemeinschaft (DFG) through the clusters of excellence "Center for Ultrafast Imaging" (CUI, EXC 1074, ID 194651731) and "Advanced Imaging of Matter" (AIM, EXC 2056, ID 390715994).

References

1 C. F. Roos M. Chwalla, K. Kim, M. Riebe, and R. Blatt, 'Designer atoms' for quantum metrology, *Nature* **443**, 316–319 (2006).

2 S. S. Kondov, C.-H. Lee, K. H. Leung, C. Liedl, I. Majewska, R. Moszynski, and T. Zelevinsky, Molecular lattice clock with long vibrational coherence, *Nat. Phys.***15**, 1118–1122 (2019).

3 G. Herzberg, Quadrupole Rotation-Vibration Spectrum of the Hydrogen Molecule. *Nature,* **163**, 170–170 (1949).

4 L. S. Rothman and A. Goldman, Infrared electric quadrupole transitions of atmospheric oxygen, *Applied Optics*, **20**, 2182- 2184 (1981).

5 A. Campargue, S. Kassi, K Pachucki, and J. Komasa, The absorption spectrum of H_2: CRDS measurements of the (2-0) band, review of the literature data and accurate *ab initio* line list up to 35 000 cm^{-1}, *Phys. Chem. Chem. Phys.***14**, 802 (2012).

6 A. Goldman, J. Reid, and L. S. Rothman, Identification of electrical quadrupole O_2 and N_2 lines in the infrared atmospheric absorption spectrum due to the vibration–rotation fundamentals, *Geophys. Res. Lett.***8**, 77–8 (1981).

7 K. H. Baines, M. E. Mickelson, L. E. Larson, D. W. Ferguson, The abundances of methane and ortho/para hydrogen on Uranus and Neptune: Implications of New Laboratory 4-0 H2 quadrupole line parameters, *Icarus* **114**, 328–340 (1995).

8 A. D. Ludlow M. M. Boyd, Jun Ye, E. Peik, and P. O. Schmidt, Optical atomic clocks, *Rev. Mod. Phys.***87**, 637 (2015).

9 J. C. Berengut, V. A. Dzuba, and V. V. Flambaum, Enhanced Laboratory Sensitivity to Variation of the Fine-Structure Constant using Highly Charged Ions, *Phys. Rev. Lett.***105**, 120801 (2010).

10 T. Pruttivarasin, M. Ramm, S. G. Porsev, I. I. Tupitsyn, M. S. Safronova, M. A. Hohensee, and H. Häffner, Michelson–Morley analogue for electrons using trapped ions to test Lorentz symmetry, *Nature* **517**, 592–595 (2015).

11 M. Quack, J. Stohner, and M. Willeke, High-Resolution Spectroscopic Studies and Theory of Parity Violation in Chiral Molecules, *Annu. Rev. Phys. Chem.* **59**, 741-769 (2008).

12 H. Haeffner, C.F. Roos, and R. Blatt, Quantum computing with trapped ions, *Physics Reports* **469**, 155-203 (2008).

13 A. D. Buckingham, R. L. Disch, D. A. Dunmur, The Quadrupole Moments of Some Simple Molecules, *J. Am. Chem. Soc.*, **90**, 3104-3107 (1968).

14 I. E. Gordon *et al.*, The HITRAN2016 molecular spectroscopic database, *J. Quant. Spectrosc. Radiat. Transfer*. **203**, 3-69 (2017).

15 O. L. Polyansky, N. F. Zobov, I. I. Mizus, L. Lodi, S. N. Yurchenko, J. Tennyson, A. G. Császár, and O. V. Boyarkin, Global spectroscopy of the water monomer, *Phil. Trans. Royal Soc. London A*, **370**, 2728-2748 (2012).

16 B. A. Fomin and V. A. Falaleeva, Recent progress in spectroscopy and its effect on line-by-line calculations for the validation of radiation codes for climate models, *Atmos. Ocean. Opt.* **22**, 626 (2009)

17 D. Romanini, A. A. Kachanov, N. Sadeghi, and F. Stoeckel, CW cavity ring down spectroscopy, *Chemical Physics Letters*, **264**, 316–322 (1997).

18 S. Kassi. and A. Campargue. Cavity Ring Down Spectroscopy with 5×10^{-13} cm^{-1} sensitivity, *J. Chem. Phys.*, **137**, 234201 (2012).

19 S. Kassi, I.E. Gordon, and A. Campargue, First detection of transitions in the second quadrupole overtone band of nitrogen near 1.44 μm by CW-CRDS with 6×10^{-13} cm^{-1} sensitivity, *Chem. Phys. Lett.* **582** 6–9(2013).

20 S. N. Mikhailenko, S. Kassi, D. Mondelain, R. R. Gamache, and A. Campargue, A spectroscopic database for water vapor between 5850 and 8340 cm^{-1}, *J. Quant. Spectrosc. Radiat. Transfer*. **179**, 198-216 (2016).

21 O. Leshchishina, S. Mikhailenko, D. Mondelain, S. Kassi, and A. Campargue, An improved line list for water vapor in the 1.5 μm transparency window by highly sensitive CRDS between 5852 and 6607cm^{-1}, *J. Quant. Spectrosc. Radiat. Transfer*. **130**, 69-80 (2013).

22 A. Campargue, S. N. Mikhailenko, B. Guillo Lohan, E. V. Karlovets, D. Mondelain, and S. Kassi, The absorption spectrum of water vapor in the 1.25 μm atmospheric window (7911 – 8337 cm^{-1}), *J. Quant. Spectrosc. Radiat. Transfer*. **157**, 135-52 (2015).

23 S. N. Yurchenko, W. Thiel, and P Jensen, Theoretical ROVibrational energies (TROVE): A robust numerical approach to the calculation of rovibrational energies for polyatomic molecules, *J. Mol. Spectrosc.*, **245**, 126-140, (2007).

24 S. N. Yurchenko, A. Yachmenev, and R. I. Ovsyannikov, Symmetry adapted ro-vibrational basis functions for variational nuclear motion: TROVE approach, *J. Chem. Theory Comput.*, **13**, 4368-4381 (2017).

25 I. I. Mizus, A A. Kyuberis, N. F. Zobov, Vl. Yu. Makhnev, O. L. Polyansky, and J. Tennyson, High accuracy water potential energy surface for the calculation of infrared spectra, *Phil. Trans. Royal Soc. London A*, **376**, 20170149 (2018)

26 CFOUR, Coupled-Cluster techniques for Computational Chemistry, a quantum chemical program package written by Stanton J. F. et al. and the integral packages MOLECULE (Almlöf J. and Taylor P.R.), PROPS (Taylor P. R.), ABACUS (Helgaker T. et al.), and ECP routines by Mitin A.V. and van Wüllen C. For the current version, see http://www.cfour.de (2018).

27 A. Owens and A. Yachmenev, RichMol: A general variational approach for rovibrational molecular dynamics in external electric fields, *J. Chem. Phys.* **148**, 124102 (2018).

28 J. Tennyson. *et al.*, IUPAC critical evaluation of the rotational-vibrational spectra of water vapor. Part III: Energy levels and transition wavenumbers for $H_2{}^{16}O$, *J. Quant. Spectrosc. Radiat. Transfer*. **117**, 29-58 (2013).

29 See Supplemental Material at [URL will be inserted by publisher] for the calculated electric-quadrupole line list of $H_2{}^{16}O$.

30 E. K. Conway, A. A. Kyuberis, O. L. Polyansky, J. Tennyson, and N. F. Zobov, A highly accurate *ab initio* dipole moment surface for the ground electronic state of water vapour for spectra extending into the ultraviolet, *J. Chem. Phys.* **149**, 084307 (2018).

31 J. Tennyson *et al.*, The ExoMol database: Molecular line lists for exoplanet and other hot atmospheres, *J. Mol. Spectrosc.*, **327**, 73-94 (2016).

32 E. S. F. Berman, N. E. Levin, A. Landais, S. Li, and T. Owano, Measurement of Δ18O, Δ17O, and 17O-Excess in Water by off-Axis Integrated Cavity Output Spectroscopy and Isotope Ratio Mass Spectrometry, *Analytical Chemistry* 85 (21): 10392–98 (2013). https://doi.org/10.1021/ac402366t.

33 E. R.Th. Kerstel and H.A.J. Meijer, Optical Isotope Ratio Measurements in Hydrology (Chapter 9), in: Isotopes in the Water Cycle: past, present and future of a developing science. pp. 109-124, P.K. Aggarwal, J. Gat, and K. Froehlich (Eds.), IAEA Hydrology Section, Kluwer, 2005.

34 J. B. McManus, D. D. Nelson, and M. S. Zahniser, Design and Performance of a Dual-Laser Instrument for Multiple Isotopologues of Carbon Dioxide and Water, *Optics Express* 23 (5): 6569 (2015). https://doi.org/10.1364/OE.23.006569.

35 E. J. Steig, V. Gkinis, A. J. Schauer, S. W. Schoenemann, K. Samek, J. Hoffnagle, K. J. Dennis, and S. M. Tan, Calibrated High-Precision $^{17}O_{Excess}$ Measurements Using Laser-Current Tuned Cavity Ring-down Spectroscopy, *Atmospheric Measurement Techniques Discussions* **6** (6): 10191–229 (2013). https://doi.org/10.5194/amtd-6-10191-2013.

36 L. Moretti, A. Castrillo, E. Fasci, M. D. De Vizia, G. Casa, G. Galzerano, A. Merlone, P. Laporta, and L. Gianfrani, Determination of the Boltzmann constant by means of precision measurements of line shapes at 1.39 μm, *Phys. Rev. Lett.*, **111**, 060803 (2013).

37 T.H. Dunning, Gaussian basis sets for use in correlated molecular calculations. I. The atoms boron through neon and hydrogen, *J. Chem. Phys.***90**, 1007 (1989).

38 R. A. Kendall, T. H. Dunning, Jr., and R. J. Harrison, Electron affinities of the first-row atoms revisited. Systematic basis sets and wave functions, *J. Chem. Phys.* **96**, 6796-6806 (1992).

39 G. E. Scuseria, E, Analytic evaluation of energy gradients for the singles and doubles coupled cluster method including perturbative triple excitations: Theory and applications to FOOF and Cr_2, *J. Chem. Phys.* **94**, 442–447 (1991).

40 S. Carter S., N. C. Handy, and B.T. Sutcliff, A variational method for the calculation of rovibrational levels of any triatomic molecule, *Mol. Phys.*, **49**, 745–748 (1983).

41 B.T. Sutcliffe and J. Tennyson, A general treatment of vibration-rotation coordinates for triatomic molecules, *Intern. J. Quantum. Chem.*, **39**, 183-196 (1991).

42 I. I. Mizus, A A. Kyuberis, N. F. Zobov, Vl. Yu. Makhnev, O. L. Polyansky, and J. Tennyson, High accuracy water potential energy surface for the calculation of infrared spectra, *Phil. Trans. Royal Soc. London A*, **376**, 20170149 (2018)

43 J. Tennyson and S. N. Yurchenko, The ExoMol project: Software for computing large molecular line lists, *Intern. J. Quantum Chem.*, **117**, 92-103 (2017).

44 J. W. Cooley, An improved eigenvalue corrector formula for solving the Schrödinger equation for central fields, *Math. Comp*. **15**, 363–374 (1961).

45 B. V. Noumerov, A method of extrapolation of perturbations, *Mon. Not. R. Astron. Soc*. 84, 592–602 (1924).

46 S.N. Yurchenko and T. Mellor, *in preparation*, (2020).

47 J. Tennyson *et al.*, The ExoMol database: Molecular line lists for exoplanet and other hot atmospheres, *J. Mol. Spectrosc.*, **327**, 73-94 (2016).

48 A. Yachmenev, L. V. Thesing, and J. Küpper, Laser-induced dynamics of molecules with strong nuclear quadrupole coupling, *J. Chem. Phys.* **151**, 244118 (2019); https://doi.org/10.1063/1.5133837